Effects of wind farm foundations on the water exchange between North Sea and Baltic Sea – A first careful assessment derived from the QuantAS-Off project

Hans Burchard[1], Frank Hüttmann[2], Frank Janssen[1,4], Hans Ulrich Lass[1], Alfred Leder[2], Mark Markofsky[3], Peter Menzel[2], Volker Mohrholz[1], Hannes Rennau[1], Stefan Schimmels[3], Lars Umlauf[1]

1. Leibniz Institute for Baltic Sea Research Warnemünde, Seestraße 15, D-18119 Rostock, Germany
2. University of Rostock, Chair of Fluid Mechanics, Albert-Einstein-Straße 2, D-18051 Rostock, Germany
3. Leibniz University of Hannover, Fluid Mechanics Institute, Appelstraße 9a, D-30167 Hannover, Germany

Abstract

In this coordinator report from the QuantAS-Off project funded by the German Federal Ministry for the Environment, Nature Conservation and Nuclear Safety (BMU) preliminary results are summarised. First, the sensitivity and ecological role of the water exchange between the North Sea and the Baltic Sea is discussed. Results for the natural variability and mixing are presented, derived from detailed field and model studies carried out within QuantAS-Off and another project within the QuantAS project cluster. It is shown that the dynamics of Baltic Sea inflow events is far more complex and variable than assumed before. Major focus is set on the quantification of the impact of structures such as cylinders (from wind turbine foundations) on the inflowing dense water masses. These studies are based on laboratory measurements (University of Rostock), local numerical simulations (University of Hannover) and field observations near obstacles in the Baltic Sea (Baltic Sea Research Institute). Then, a parameterisation of structure mixing for large scale regional hydrostatic ocean models is suggested, based on a quadratic friction law. Strategies for calibration are discussed. Finally, mainly based on the local simulations by the University of Hannover, a first quantification of mixing due to wind farms is attempted. The result is that wind farms, depending on their location, may have a dynamic influence on the exchange between the North Sea and the Baltic Sea, but that the uncertainties are still too large to give definitive estimates. During the last phase of the QuantAS-Off project, the three project partners will further cooperate to improve the predictability for structure induced mixing. This work will mainly be based on improving the structure friction parameterisation by calibrating it against the laboratory simulations and local numerical simulations and then carrying out regional model simulations for the Western Baltic Sea with this parameterisation implemented, considering a variety of wind farm distributions.

1 Introduction

1.1 Ecological role of Baltic inflow events

Due to its topography with narrow and shallow connections to the world ocean (via Kattegat, Skegarak and the North Sea) in the western part and with its relatively deep basins further east

[4]now at: Federal Maritime and Hydrographic Agency, Bernhard-Nocht-Straße 78, D-20359 Hamburg, Germany

(see figure 1), the Baltic Sea ecosystem is specifically vulnerable. Due to the permanent stable stratification of the Baltic Sea, resulting from a balance of freshwater supply from rivers and atmospheric precipitation and salt water supply from the North Sea, the deeper parts of the basins are cut off from direct mixing with surface waters. Degradation of dead organic matter sunk down to the deeper waters leads to substantial oxygen demand in those areas. During stagnation periods, i.e. between major salt water inflows into the Baltic Sea, large areas of the Baltic Sea deep water may be depleted from oxygen, not allowing presence of any higher life forms. Additionally, high amounts of phosphate are released from sediments under oxygen-depleted water masses, which favour, after been mixed up into the euphotic zone near the sea surface, massive summer blooms of toxic cyanobacteria.

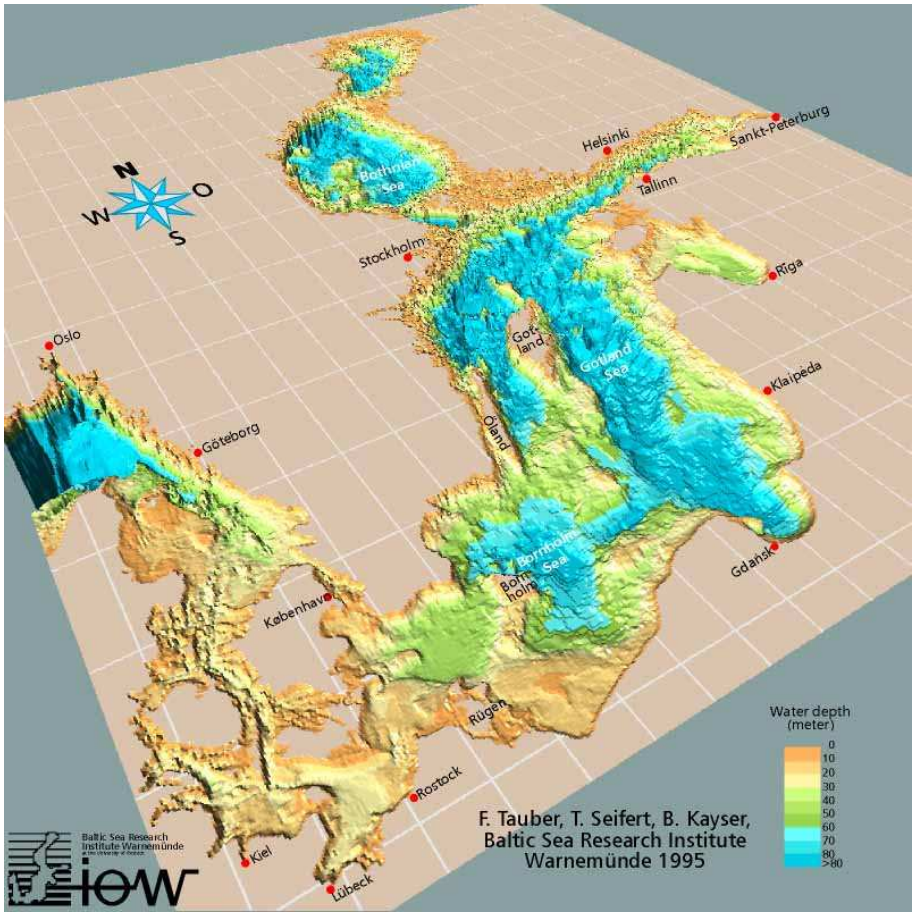

Figure 1: Bathymetry of the Baltic Sea. The figure has been copied from the website `www.io-warnemuende.de`.

With this, the important role of inflow events from the North Sea, bringing waters with relative high oxygen concentrations to the deeper basins of the Baltic Sea is clear. On their way through the narrow approaches into the Baltic Sea, these inflows, which creep along the sea bed, finding

their way over the sills and channels, are subject to strong natural mixing. With typical salinities of 20-25 g/kg when entering the Arkona Sea, their salinity drops to under 14 g/kg at the bottom of the Gotland basin. This is entirely due to entrainment of lower salinity waters from above, driven by turbulent mixing. The stronger the entrainment is, the smaller is the potential of these inflows to reach the deeper parts of the deeper basins. The inflows need to have a higher density (which for the Baltic Sea is largely proportional to the salinity) than the bottom water in order to be able to creep under those and push them away, thus ventilating the deeper basins. The turbulent mixing processes leading to the Baltic Sea vertical overturning circulation, of which the inflow events are a substantial part, is shown in figure 2.
This turbulent mixing and entrainment is a natural process which however is little understood yet. Quantifications for this have not yet lead to conclusive results. Furthermore, human constructions in the pathway of the inflowing saline waters in the region of the Western Baltic Sea have the potential to additionally mix these bottom waters. Such constructions may be piles of bridges, artificial islands or foundations of offshore wind turbines. Also mixing by ship traffic in shallow water may significantly contribute to the mixing.

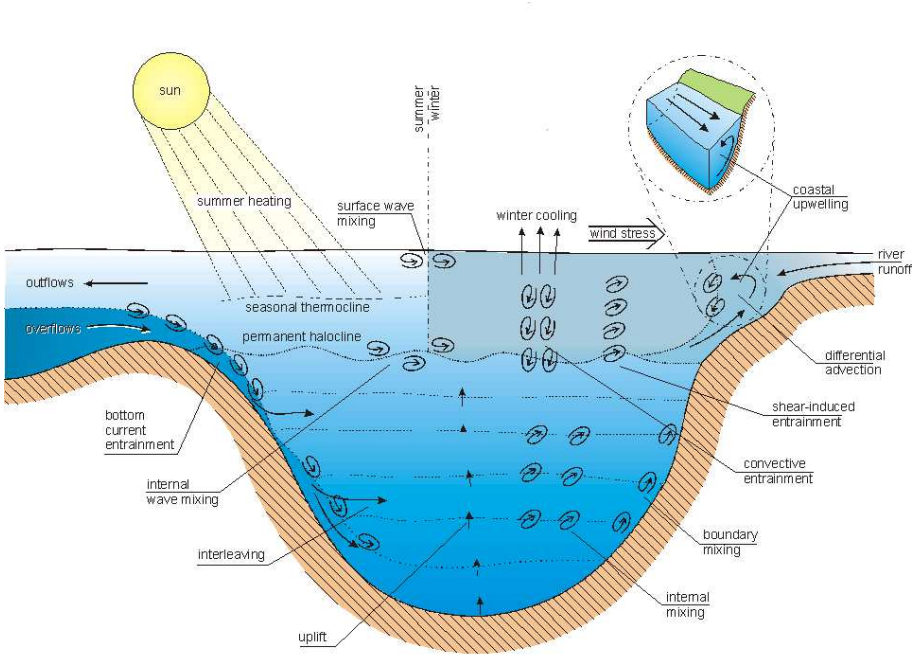

Figure 2: Scheme of vertical mixing and transport processes in the Baltic Sea. This figure has been taken from Reissmann et al. (2008).

1.2 Objectives of the QuantAS projects

In order to quantify the natural and anthropogenic mixing of Baltic Sea inflow events, an international consortium of oceanographers has been established, with members from Germany,

Denmark, Poland and Sweden. The aim of the consortium is to jointly carry out research in support of unravelling the mixing processes in the Western Baltic Sea. The initiative has been named QuantAS, which stands for *Quantification of Mater Mass Transformations in the Arkona Sea*. Two German projects have been proposed, QuantAS-Nat for studying natural mixing (funded by the German Research Foundation, 2005-2009), and QuantAS-Off for studying the potential effect of offshore wind farms (funded by the German Federal Ministry for the Environment, Nature Conservation and Nuclear Safety, 2005-2009). Both projects are closely interlinked, with QuantAS-Off being a project cluster including projects at the Leibniz Institute for Baltic Sea Research in Warnemünde, the Chair of Fluid Mechanics at the University of Rostock and the Fluid Mechanics Institute of the Leibniz University of Hannover.
According to the QuantAS-Off proposal, key questions to be answered are:

- How much will dense and oxygen-rich bottom currents through the Arkona Sea into the Baltic Sea be obstructed and diluted by underwater constructions such as foundations of offshore wind farms ?

- Which influence do these water mass transformations have on the flux (and its distribution) of oxygen-rich North Sea water into the basins of the Baltic Sea such as the Bornholm Basin and the Gotland Basin ?

- Which recommendations for the location, layout and extent of off-shore wind farms can be given to the authorities responsible for approving the erection of offshore wind farms ?

The approach to answer these complex questions is to construct a proper parameterisation of mixing of inflow events tailor-made for the Baltic Sea and to carry out a number of numerical experiments for the Western Baltic Sea with this parameterisation implemented.
The logical structure of the QuantAS-Off project is shown in figure 3.
These parameterisations would have to fit into hydrostatic models for the Western Baltic Sea, i.e. into models which are able to reproduce the dynamics of the Western Baltic Sea over periods of several years, but do not resolve the smaller scales (such as whirls behind structures in stratified flow). The calibration of such parameterisations is one of the most complicated tasks within the project, since so far, the dense bottom currents itself have not been fully understood. Therefore, first of all, QuantAS-Off needed to be strongly interconnected with QuantAS-Nat, for understanding the natural processes, see work package 1 in figure 3 and section 2 for main results. Secondly, the interaction between stratified (and sheared) currents with structures needed to be studied in detail. For this central part, a strategy based on three experimental setups has been chosen (see work package 2 in figure 3):

- Small-scale laboratory experiments carried out by the University of Rostock (WP 2.1), for details, see section 3.1).

- Small-scale numerical experiments carried out by the University of Hannover (WP 2.2), for details, see section 3.2).

- Small-scale in-situ observations of structure induced mixing carried out by the Leibniz Institute for Baltic Sea Research (WP 2.3), for details, see section 3.3).

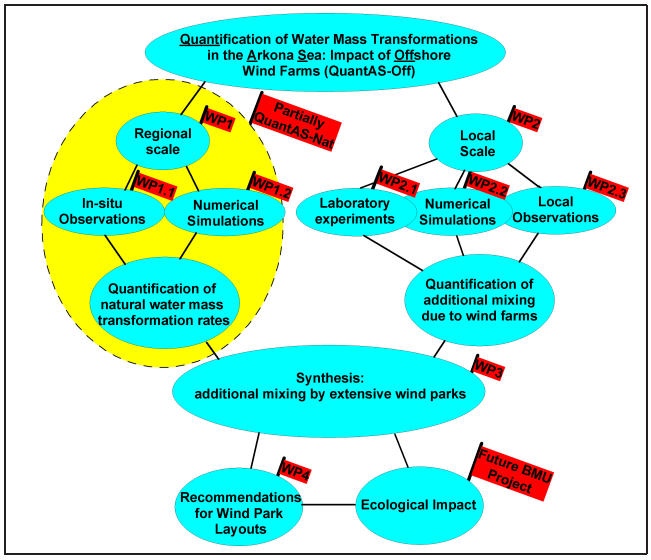

Figure 3: Diagram showing the organisation of QuantAS-Off and its relation to other future projects.

Once these parameterisations have been developed and calibrated, they will be implemented into the model for the Western Baltic Sea in order to quantify the additional mixing effects of wind farms by comparing model results with and without wind farm parameterisation.
In the final work package 4, numerical experiments will be carried out with various wind farm densities and distributions for giving recommendations for future planning.

1.3 General properties of Baltic inflows

Major Baltic inflow events are known as the only process for the ventilation of the Baltic Sea deep waters (Wyrtki (1954), Matthäus and Frank (1992), Lass and Matthäus (1996), Lehmann et al. (2004), Feistel et al. (2006), Reissmann et al. (2008)). In recent years, major barotropic inflows, driven by a substantial sea level difference between the Kattegat and the Baltic Sea and persistent westerly winds, occurred in 1983, 1993 and 2003. Exceptionally strong baroclinic inflows, driven by the horizontal density gradient between the Kattegat and the Baltic Sea have been observed during the summers of 2002 and 2003 (Feistel et al. (2003), Feistel et al. (2004)). These fairly rare, but significant events which mostly enter the Baltic Sea over the Belt Sea and Darss Sill and typically change the hydrography in the deep waters of the Gotland basin, have always gained a lot of awareness.
However, smaller inflow events, which typically enter the Baltic Sea first and most effectively via the Øresund and the Drogden Sill (see figure 4 for coastlines, bathymetry and geographical names), occur several times per year and are vital for the ventilation of intermediate layers in the Bornholm Basin, are of similar importance. Such medium intensity inflow events are essential for the maintenance of a suitable habitat for cod egg development in the halocline area of the Bornholm Basin (Mohrholz et al. (2006)). On their way over the sills through the Arkona

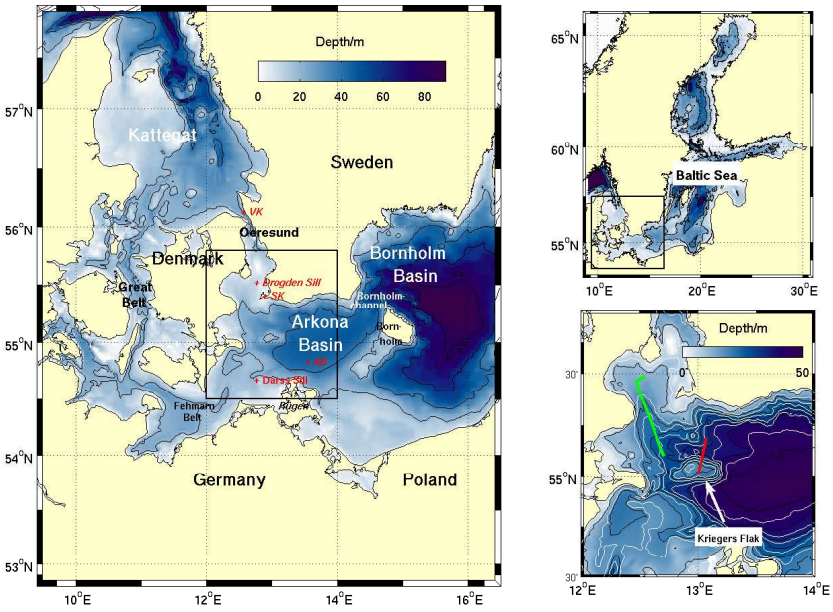

Figure 4: Map of the Baltic Sea showing the domain of the Baltic Sea model (upper right panel), the domain of the Western Baltic Sea model (left panel) and the area of the Drogden Sill and Kriegers Flak area (lower right panel). The latter map shows the cross-sections which have been observed during a field campaign on February 1 (green) and February 5 (red). The positions of the Drogden Sill, Darss Sill (DS) and Arkona Buoy (AB) stations are shown in the left map as well as the locations of the coastal gauges in Viken (VK) and Skanör (SK). The Baltic Sea model has an open boundary in the Skagerak at 9°E, and the Western Baltic Sea model has open boundaries between Kattegat and Skagerak at 57°30'N and east of the Bornholm Sea at 16°30'E.

Basin over the Bornholm Channel and into the Bornholm Basin, the medium intensity inflows propagate as dense bottom currents, and are thus subject to entrainment of overlaying brackish waters which reduce their density and thus decrease the density of the isopycnal surface at which they sandwich into the halocline of the Bornholm Basin. Kõuts and Omstedt (1993) analysed from long term hydrographic observations that the volume of dense bottom water increases by 53% due to entrainment in the Arkona Basin. Lass and Mohrholz (2003) hypothesised that the major mixing mechanism is differential advection (denser water sheared over fresher water) in the front region of the intermittent dense bottom currents and estimated a mixing related volume increase of dense bottom water by 30% for the passage from Drogden Sill to the Bornholm Channel. Liljebladh and Stigebrandt (1996) and Lass and Mohrholz (2003) investigated in detail the pool state of the Arkona Basin, during which a large amount of dense water is passively stored as a few metre thick layer in the eastern flat-bottom part of the Arkona Basin. There, the dense water is subject to mixing processes such as diapycnal mixing, upwelling and wind

entrainment (Lass and Mohrholz (2003)).

2 Results for natural mixing

All observational efforts for quantifying the mixing in the Arkona Basin are substantially limited by the intermittency of the dynamics and the subsequent spatial and temporal undersampling. In fact, until before the QuantAS consortium had been established, the propagation of medium intensity inflow events has not been directly observed. It was by idealised numerical model simulations that the pathways of Drogden Sill inflow events have first been hypothesised. By using different numerical models, and in contrast to the assumptions of Lass and Mohrholz (2003), Burchard et al. (2005) and Lass et al. (2005) found that the preferred pathway of such dense bottom currents should be southward from the Drogden Sill, with a turn to the east at about 55°10'N, such that the saline water flows along the channel north of Kriegers Flak from where it enters the dense bottom pool in the eastern Arkona Basin. Observations in January/February 2004 indeed confirmed this predicted behaviour (Burchard et al. (2005), Sellschopp et al. (2006)). Umlauf et al. (2007) and Reissmann et al. (2008) present more recent cross-sectional high-resolution observations of a dense bottom current propagating eastwards north of Kriegers Flak, including data for temperature, salinity, current speed and direction, and the turbulent dissipation rate. Examples for this complex transverse structure are shown in figure 5. These observations reveal a distinct transverse circulation pattern as it has been observed by Paka et al. (1998) for the Stolpe Furrow east of the Bornholm Basin. It is obvious from the observations by Umlauf et al. (2007) that turbulent entrainment is significantly modified by this transverse structure of the dense bottom current.

The potential of numerical models to reproduce the Arkona Basin dynamics in a qualitatively and quantitatively satisfying way has been demonstrated by Burchard et al. (2005) and Arneborg et al. (2007). The latter successfully applied a one-dimensional water column model for simulating observations of current, density and turbulence at a 19-hour station in the dense bottom current north of Kriegers Flak.

For the QuantAS projects, Burchard et al. (2008) used the General Estuarine Transport Model (GETM, see `www.getm.eu` and Burchard and Bolding (2002)) for simulating the dynamics of the Western Baltic Sea during 9 months between September 2003 and May 2004, including the period of the field observations (first QuantAS cruise) obtained on early February 2004, as documented by Sellschopp et al. (2006). Since observations of boundary values cannot be obtained in high enough quality, the boundary conditions for the Western Baltic Sea model needed to be generated by the larger scale Modular Ocean Model (MOM-3.1, see Griffies et al. (2001) for the general numerical model and Neumann et al. (2002) and Janssen et al. (2004) for Baltic Sea applications). The Baltic Sea MOM-3.1 model was applied with a horizontal resolution of 3 nm and 77 vertical (geopotential) grid layers, with a near-surface resolution of 2 m, increasing with depth. The simulation was initialised with temperature and salinity analysed from observations (see Meier et al. (1999)) on May 1, 2002, and forced with surface meteorology from ECWMF Reanalysis Project ERA40 with a resolution of 100 km and 6 hours (until August 2002) and the German Weather Service Global Model with a resolution of 60 km and 6 hours (from September 2002). From the large scale Baltic Sea simulation, surface elevations at the

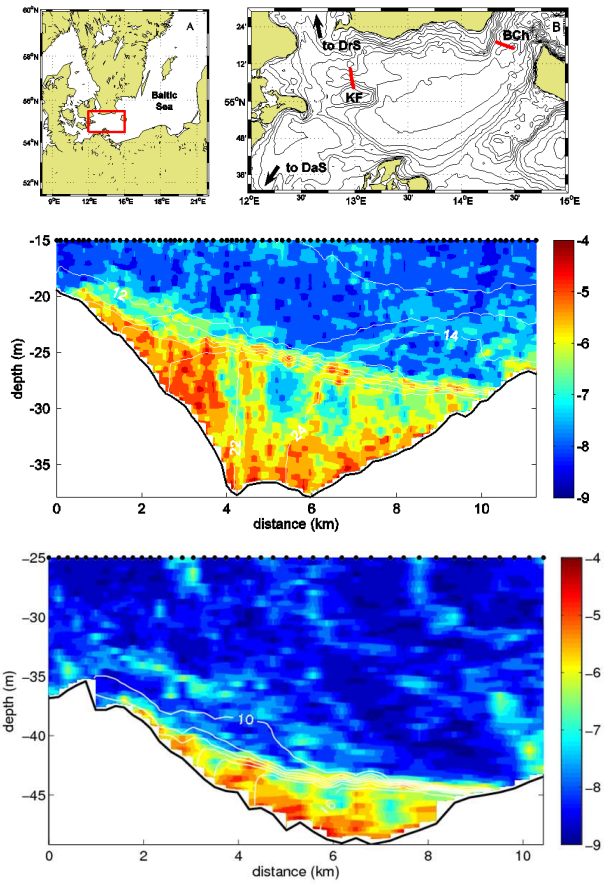

Figure 5: Upper panel: Map of the western Baltic Sea covering the Arkona Basin. Indicated in red are the transects north of Kriegers Flak (KF) and across the Bornholm Channel (BCh), shown below. Middle panel: Meridional transect across the channel north of Kriegers Flak, on November 17, 2005. Shown are contours of salinity in g/kg. The colour scale indicates the decadal logarithm of the viscous dissipation in W/kg. Lower panel: As middle panel, for a transect across the north-western part of the Bornholm Channel, on November 19, 2005. This figure has been taken from Reissmann et al. (2008).

open boundaries of the Western Baltic Sea model (between Kattegat and Skagerak at 57°30'N and east of the Bornholm Basin at 16°30'E) are stored every 15 min. for the surface elevation and every hour for temperature and salinity. The Western Baltic Sea simulation (see figure 4 for the bathymetry) was then initialised on September 1, 2003, with temperature and salinity interpolated from the Baltic Sea model, and was forced with the German Weather Service Local Model with a resolution of 7 km and 3 hours. Lateral boundary conditions were interpolated from the Baltic Sea model as discussed above. The model resolution was 1/2 nm in the horizontal, and 50 general vertical coordinate layers, with a non-linear zooming towards the bed.
Some bathymetry adjustment has been carried out in such a way, that the barotropic flow through the Øresund as well as the baroclinic flow across Darss Sill have been optimised. Figure 6 shows that the simulated salinities over Darss Sill agree well with the observations. The vertical structure of inflow events is reproduced by the the model simulations. Other validation stations have been the Drogden Sill and the Arkona Buoy, for which the observations could be reproduced as well, for details, see Burchard et al. (2008).

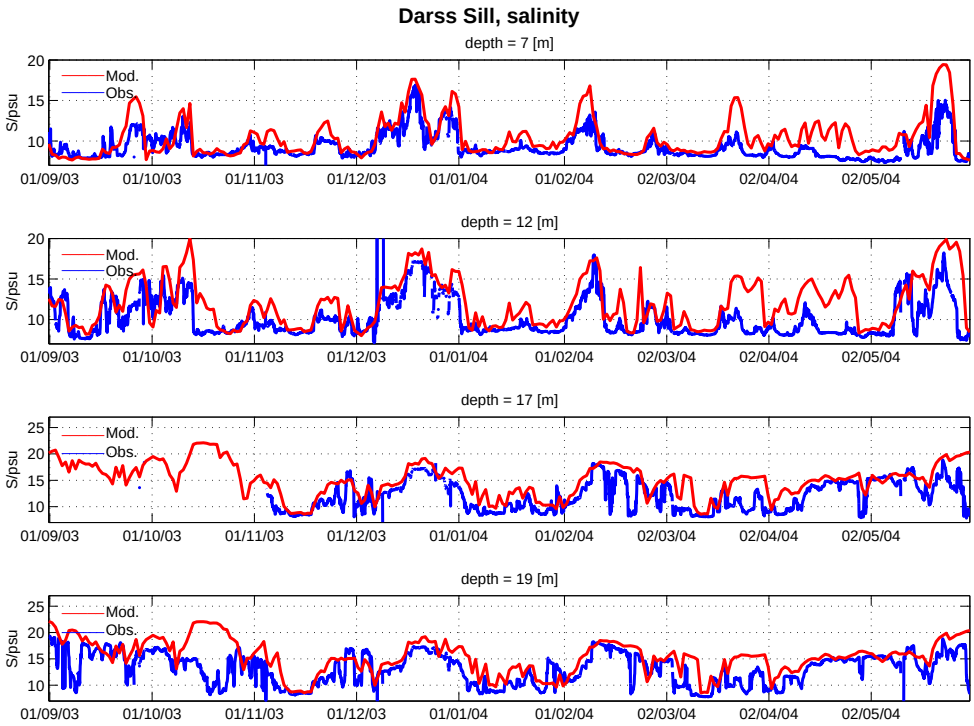

Figure 6: Time series of salinity at the Darss Sill mast. Blue: observations, red: model results. Shown are data at 7 m, 12 m, 17 m and 19 m below the mean sea level. The mean water depth at this station is 20 m. This figure has been taken from Burchard et al. (2008).

The simulated passage of the Drogden Sill overflow north of Kriegers Flak in early February 2004 is compared to model simulation results for February 7, see figure 7. This time shift was necessary in order to account for effects of model inaccuracies in terms of forcing and bathymetry,

resulting in a wrong position of the Kattegat front before the inflow. With the Kattegat front displaced too far to the north, high salinity waters reach the Drogden Sill too late after the onset on an inflow event. In figure 7, we see the cross-sectional plume structure which has already been discussed for that position in more detail by Burchard et al. (2005), Sellschopp et al. (2006) and Umlauf et al. (2007). The plume is to first order geostrophically adjusted and leaning towards the northern slope of Kriegers Flak, and in good agreement with the observations shown by Sellschopp et al. (2006).

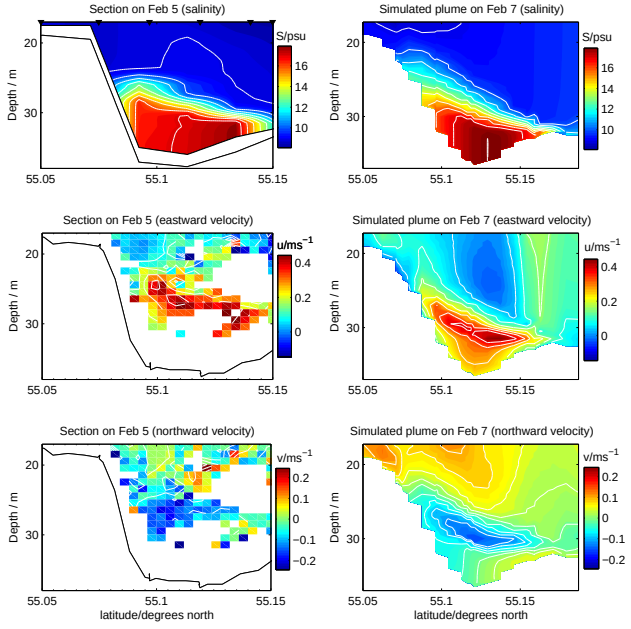

Figure 7: Observed (left) and simulated (right) salinity and current velocity on a north-south transect across the channel north of Kriegers Flak, deduced from CTD profiles and Acoustic Doppler Current Profiler. The observations were taken on February 5 from 10:45 h - 12:30 h (UTC). The black triangles in the upper left panel show the positions of the single CTD profiles. These salinity and current velocity data have been obtained by FWG Kiel, Germany (see Burchard et al. (2005) and Sellschopp et al. (2006)). This figure has been taken from Burchard et al. (2008).

After the model simulations for the Western Baltic Sea have been validated, the model results may be analysed. This has been done by Burchard et al. (2008) in some detail for the mixing. For better quantification of mixing, a new estimate for the mixing has been introduced by Burchard et al. (2008). Instead of using the vertical salt flux as measure, the decay of salinity variance due to physical mixing has been defined, which (vertically integrated over the water column) is of the following form:

$$P_T^{int} = 2 \int_{-H}^{\eta} \nu_t^S (\partial_z \bar{S})^2 \mathrm{d}z, \tag{1}$$

with the salinity S, the eddy diffusivity ν_t^S, the mean water depth H and the sea surface elevation η. This formulation has the advantage of being physically far more reasonable than the vertical turbulent salt flux.

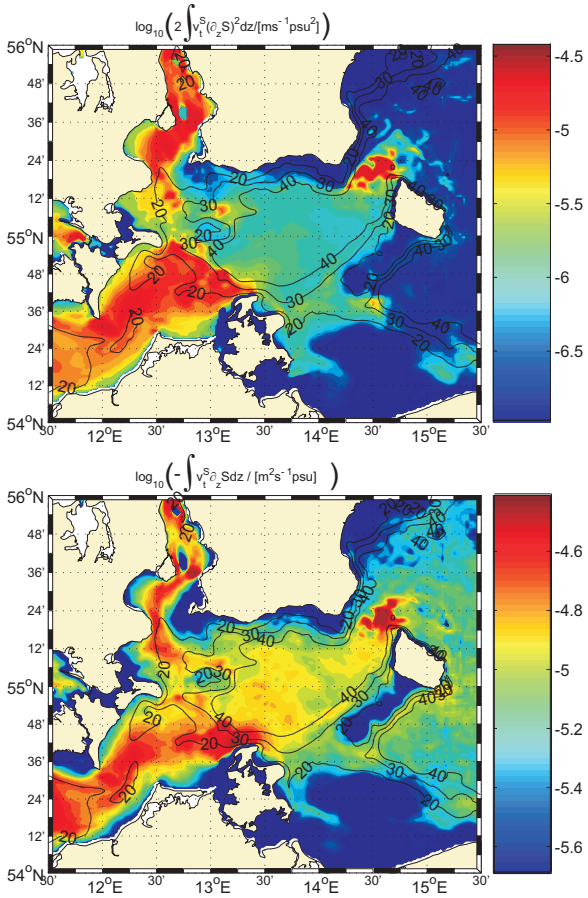

Figure 8: Simulated decadal logarithm of vertically integrated salinity variance dissipation, $\log_{10}\left(2\int \nu_t'(\partial_z S)^2 \mathrm{d}z\right)$ in $[\mathrm{m\,s^{-1}psu^2}]$ (upper panel) and decadal logarithm of vertically integrated upward turbulent salt flux $\log_{10}\left(-\int \nu_t'\partial_z S \mathrm{d}z\right)$ in $[\mathrm{m^2 s^{-1}psu}]$ (lower panel), both temporally averaged over the nine-month simulation period.

In figure 8, the decadal logarithm of the vertically integrated decay of salinity variance and the vertically integrated upward turbulent salt flux are shown as averages over the whole nine-month model simulation period. With this, areas of generally strong mixing in the Western Baltic Sea can be identified. It can be seen from both measures that highest values occur on Drogden Sill, Darss Sill and in the Bornholm Channel as well as north-west of the island of Rügen. Furthermore, the complete dense water pathways from the sills at Drogden and Darss into the Arkona Basin are characterised by strong mixing. Levels of elevated mixing are also observed north-east of Kriegers Flak, the area covered by the dense bottom current observations shown in figure 7.

One concern of numerical modelling is always the numerical diffusion. In order to discriminate between physical and numerical mixing, Burchard and Rennau (2008) have developed a new method for quantifying numerically and physically induced mixing in a consistent way. Details are given in their publication, but the method boils down to the difference between the square of the advected salinity and the advected square of the salinity. The result for the numerical mixing in the Western Baltic Sea is surprising, see figure 9.

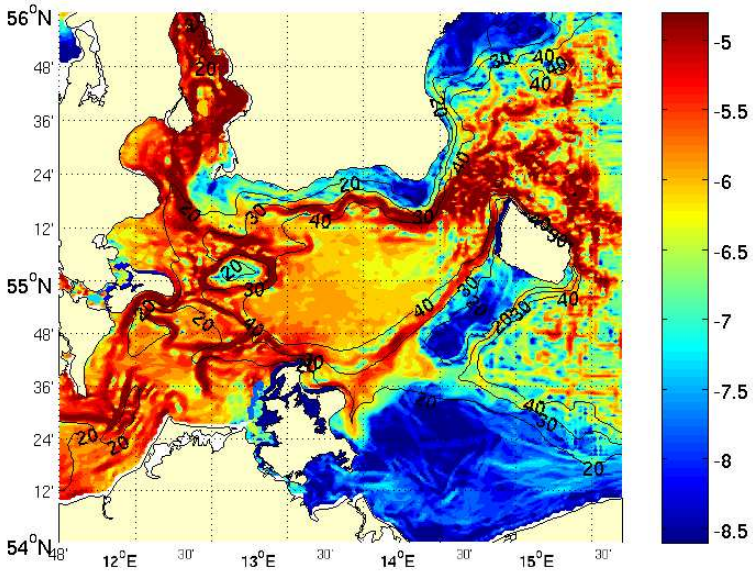

Figure 9: Decadal logarithm of vertically integrated numerically-induced salinity variance decay, as a measure for numerical mixing, temporally averaged over the nine-month simulation period.

The order of magnitude of numerically-induced mixing is comparable with the physically-induced mixing (see figure 8, upper panel), but the spatial distribution is completely different. High values occur mostly where the halocline (strong vertical salt gradient) encounters with the sloping bed, as can be clearly seen along the 35 m depth contour. Thus, when evaluating mixing in the Baltic Sea on the basis of numerical models, this numerical mixing has surely to be taken into account.

3 Estimates of mixing due to structures

3.1 Laboratory experiments

For first characterisation of the flow conditions inside the measuring section (see Menzel et al. (2006) and Menzel et al. (2007)) the vertical extension of the saltwater layer has been analysed in the section without any model as well as using the cylinder model. To achieve this vertical extension the LIF-measurements of concentration-fields have been used. We define the upper border of the saltwater layer as the position where the concentration takes 50% of the maximum.

For the laboratory experiments with a densimetric Froude-number $F_r = 0.5$ this corresponds to a salinity of 5 g/kg. The position of the 50%-line is shown in figure 10, where the red line describes the measurements without the cylinder model and the black on the measurements with the cylinder model build in. These diagrams display results that have been averaged over 1000 time steps. It is obvious that the vertical extension of the saltwater layer in the experiments without the model (red) does not change within the uncertainty of the measurements. This proves that the measuring section and the border conditions have been well chosen. Using the cylinder model (black) a sinking of the layer in the near wake of the cylinder occurs. Towards the end of the measuring section the position of the mixing layer in this case conforms to the one without the cylinder model. This result is a strong indication to declare that the cylinder has no influence on the vertical extension of the saltwater layer in large distance from the cylinder. To determine the influence of the cylinder on the mixing layer the vertical extension of the mixing layer itself has been specified. For this the vertical position of 50% of the maximum salinity as well as the vertical displacement of this point to the points of 30%, 40%, 60% and 70% of the maximum salinity have been determined. Following these quantities have been averaged over 1000 time steps for each x-position.
In figure 11 these lines are shown, where the red lines display the raw data of the measurements without cylinder model and the green lines the regression lines on these data. The black lines illustrate the raw data of the measurements with cylinder model and the blue lines the belonging regression lines. Considering the charts for 4 g/kg and 6 g/kg it becomes apparent that there is no significant influence of the cylinder model detectable under the chosen border conditions. Also the raw data of the lines reflecting 3 g/kg and 7 g/kg demonstrate no significant influence of the cylinder on the vertical extension of the mixing layer in large distance to the cylinder within the border conditions and the measuring accuracy.
For quantification of a mixing effect the volume flux of mixed water can be divided by the volume flux of saltwater at the place of the cylinder. Therefore the following relation can be used:

$$M = \frac{V_{30_{mz}}^{70} - V_{30_{oz}}^{70}}{V_0} = \frac{\int_{z(30\%)}^{z(70\%)} u_{mz}\,\mathrm{d}z - \int_{z(30\%)}^{z(70\%)} u_{oz}\,\mathrm{d}z}{\int_{-4D}^{z(50\%)} u_0\,\mathrm{d}z} \tag{2}$$

In case that the vertical distance between the lines of 30% and 70% of the maximum salinity in the far field of the cylinder increases about 1mm from the case without cylinder to the case with cylinder and the velocities u_{mz} and u_{oz} are constant with z and amount to 50% of the incident velocity u_0, then the so derived mixing amounts to 0.5%. To archive 1% mixing the vertical distance between both concentration values has to increase about 2 mm, which would be detectable within the measuring uncertainty.
The source of eventual mixing is located in the near wake of the cylinder model. From the results of Stereo-PIV-measurement a flow structure can be characterised. Figure 12 gives information about the dominant vortex structure in the wake of the cylinder. The isosurfaces of the x-component of the vorticity are red (spinning left) and blue (spinning right) coloured and clearly show a positive (upwards) velocity component at $y/d = 0$ and a negative (downwards) velocity component at $y/d = \pm 0.5$. This vortex tainted flow only takes place within the saltwater layer.

To point up this the isosurface of the salinity value of 5 g/kg (50% of the maximum salinity) is also shown. In content with the isosurfaces of the vorticity-component ω_x it can be seen that a rotation of the fluid due to the vortex structure only occurs near the bottom inside the saltwater layer. This implies that there are no measurable exchange processes between saltwater and freshwater caused by the cylinder under the chosen experimental conditions at a densimetric Froude-number $F_r = 0.5$.

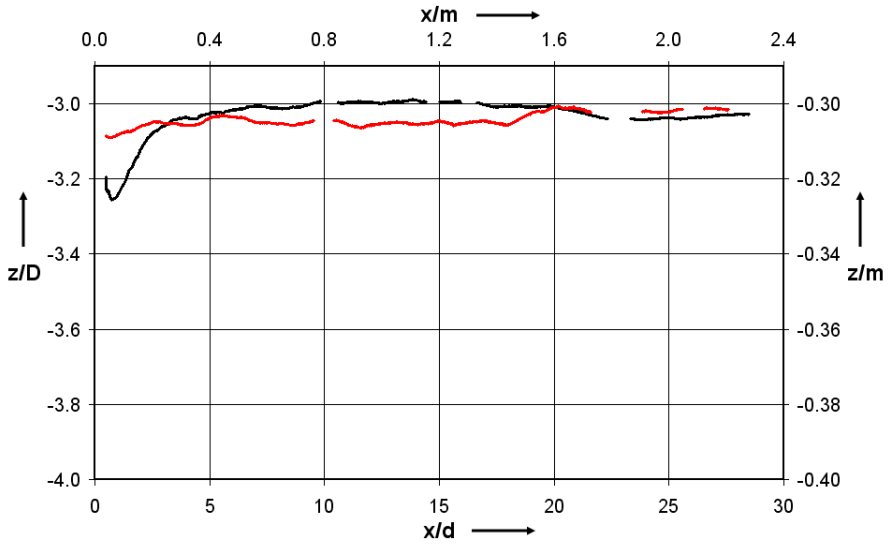

Figure 10: Vertical extension of the saltwater layer defined at a salinity of 5 g/kg. Measurements (red) without cylinder model and (black) with cylinder model.

3.2 Small-scale numerical experiments

The major goal of the work by Schimmels (2007) was the investigation of the influence of circular cylinders on density currents motivated by the desire to determine the impact of planned offshore wind energy farms on the dilution of such currents in the Baltic Sea. The approach to the problem in the present case was based on detailed three-dimensional numerical simulations with a non-hydrostatic requiring a proper definition of the issues of matter and a thorough validation of the numerical model. Special emphasis was placed on the Reynolds averaged Navier-Stokes (RANS) equations being the basis for all simulations in the present work. As it was not clear from the beginning which turbulence model is best suited for the present problem many different models were considered and thoroughly discussed.
According to the motivation of QuantAS-Off the analysis of cylinder induced mixing is based on simulations on a natural scale, motivated by the study by Arneborg et al. (2007). However, to provide the outcome of this work with a more general matter all results were evaluated and presented by means of non-dimensional parameters governing the flow. For the present problem these were identified to be the densimetric Froude number, F_r, in terms of the general stability

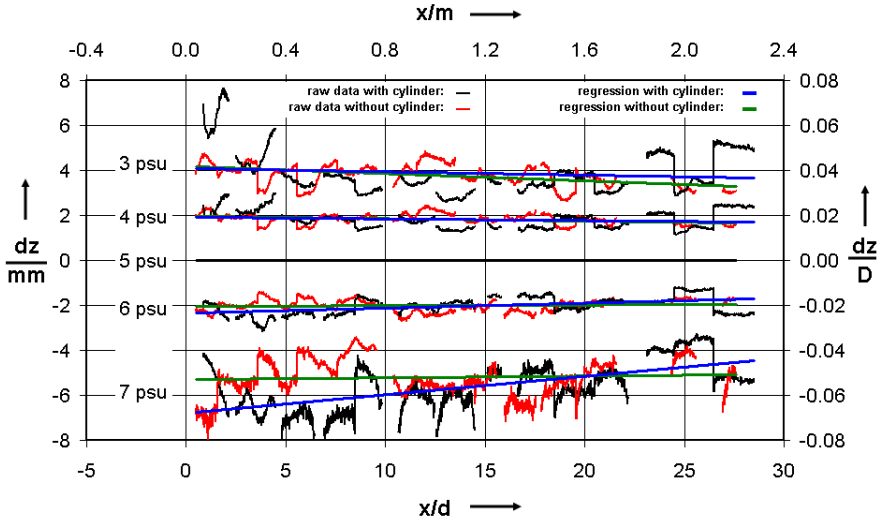

Figure 11: Vertical extension of the mixing layer. Measurements (red) without and (black) with cylinder as well as regression lines (green) without and (blue) with cylinder).

of the current, the cylinder Reynolds number, R_e, and the ratio of current depth to cylinder diameter, D/d, in terms of the flow properties around the cylinder. For the cases including Earth rotation, the Ekman number, K, could be shown to be a fourth governing parameter. However, the lateral currents induced by Coriolis forces significantly complicate the flow around the cylinder and inhibit an analysis of the principal effects. The major emphasis was therefore so far on currents without Coriolis forces and the effect of the Ekman number was so far only shortly discussed.

The influence of the governing parameters on the flow field, entrainment rates and mixing efficiencies were thoroughly investigated by means of a parameter study. As could be expected from the simulations of unstratified cylinder flow it turned out that the Reynolds number in the present order of magnitude ($R_e \approx 10^6$) is rather unimportant. While the magnitude of the Reynolds number strongly depends on the scale of the flow the Froude number and aspect ratio are scale independent and could be shown to have a certain influence on the results.

A comparison of the spatial distributions of the entrainment rates showed that the local effect of the cylinder is quite significant with entrainment rates being up to 2 orders of magnitude larger than those of an undisturbed current. However, the area of influence of the cylinder is confined and was found to be only about 20 diameters long and 6 diameters wide, more or less independent of Froude number and aspect ratio. On the other hand there is also some entrainment in front of the cylinder induced by the bow wave which showed up to change with both parameters even if it was not possible to find a clear dependence.

The global effect of the cylinder can be regarded as the total amount of additionally entrained ambient fluid found by integration of the local entrainment rates. Based on the admittedly sparse present data it was possible to provide some kind of entrainment laws for the dependence

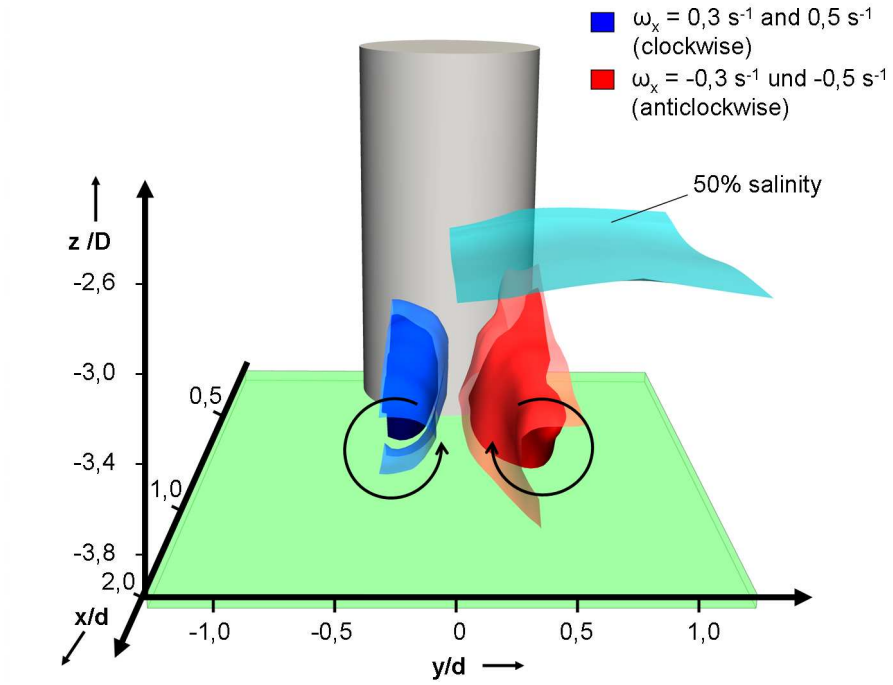

Figure 12: Isosurface of the salinity at 5 g/kg and isosurfaces of the x-component of the vorticity (red and blue).

of the total entrainment on the Froude number and aspect ratio, respectively. The law for the latter showed an exponential decrease of entrainment with increasing depth to diameter ratio while that for the Froude number was assumed to be a potential law like for undisturbed density currents with entrainment increasing with Froude number.

After the principal effects of cylinder induced mixing had been thoroughly analysed, finally the effect of Coriolis forces was shortly discussed by Schimmels (2007) and the Ekman number was introduced as a further governing parameter. The complexity of the flow field around the cylinder was presented and it could be shown that entrainment in the wake is deflected by the strong lateral currents within the interface due to the Coriolis forces.

In spite of the complex flow field and the deflection of the wake local entrainment rates and bulk flux Richardson numbers were found to be independent of the Ekman number but only depend on Froude number and aspect ratio as discussed before. Coriolis force seemed to have generally a sustaining effect on entrainment such that the area of influence of the cylinder increases with increasing Ekman number and the total entrainment also gets larger. By an example typical for a situation in the Baltic Sea it could be shown that the total impact of a cylinder is about 5 times larger due to the presence of Coriolis forces. Figure 13 shows the cross-sectional structure of the flow field for a cylinder with a diameter of half of the plume thickness. It can be clearly seen that the scale of the eddy-structures behind the cylinder is comparable to the thickness of the plume.

Figure 14 demonstrates the effect of the cylinder diameter on the entrainment. Some of the quantitative results of Schimmels (2007) are discussed in sections 4.2 and 5. For further details of the near-field numerical experiments see Schimmels (2007). However, the effect of Coriolis forces and the influence of the Ekman number were only sparsely analysed and definitely require further research.
It was the first time that the influence of cylindrical structures on mixing and entrainment in density currents has been investigated in such detail. Although the work by Schimmels (2007) provided many insights into the individual processes and allowed for a general estimate of the impact of circular cylinders on density currents, the present analysis can be regarded to be far from being complete.

3.3 Small-scale in-situ observations

Since no wind turbines are presently established in the saltwater paths of the Baltic Sea the piles of the western part of the Great Belt Link (GBL) between the Danish islands Fyn and Sprogø were chosen by Lass et al. (2008) during two cruises in January and April 2006 to study the impact of piles on a moving stratified flow. The aim of the investigations in the neighbourhood of the Western GBL was to study whether there is a vertical enhanced mixing induced by a pile in a stratified sheared flow and how enhanced mixing depends on both the background stratification and the flow. A map of the area around the Western GBL is shown in figure 15.
Between 24 January 2006 22 UTC and 25 January 2006 06 UTC several tracks with a towed CTD chain were performed parallel to the bridge on its northern and southern side, respectively. All tracks north of the bridge (upstream) depicted a general stratification with little horizontal variability, see the left panel in figure 16. Although the distance between the tracks north and south of the bridge is only about 500 m, the patterns of temperature and salinity structure of both tracks are quite different in both the general structure and the fine structure. The northern tracks were all characterised by a well mixed layer in the upper 5 to 7 m of the water column while the southern tracks all depicted a diffusive upper mixed layer suggesting that warmer saltier water was mixed from the pycnocline into the upper mixed layer. Moreover, the fine structure of the disturbances of the stratification was different from that of the northern sections as well. The characteristic fine scale pattern on the southern tracks consists of diffusive vertical elevations with increasing salinity and temperature in the surface layer and lowered salinity at the same location in the bottom layer. The characteristic horizontal scale of these disturbances is about 70 m, which is exactly the spacing of the bridge piles (see right panel in figure 16).
During the April 2006 cruise Lass et al. (2008) were able to tow a Scanfish-CTD system (observing temperature and salinity time series) in the near surface layer along a few tracks aligned in north-south direction passing the western part of the GBL in the shipping channel which is centred between two bridge piles. The first of these tracks was performed in 8 m depth close above the pycnocline while the surface current was flowing southward with 0.4 m/s. Both the mean value and the variability of salinity were quite similar at distances exceeding 100 m upstream and downstream of the bridge while close to the bridge salinity was lower and the variability enhanced, see figure 17. The tows of the CTD in the near surface layer upstream of the bridge on tracks aligned parallel to the bridge supported the results obtained with the CTD-chain mea-

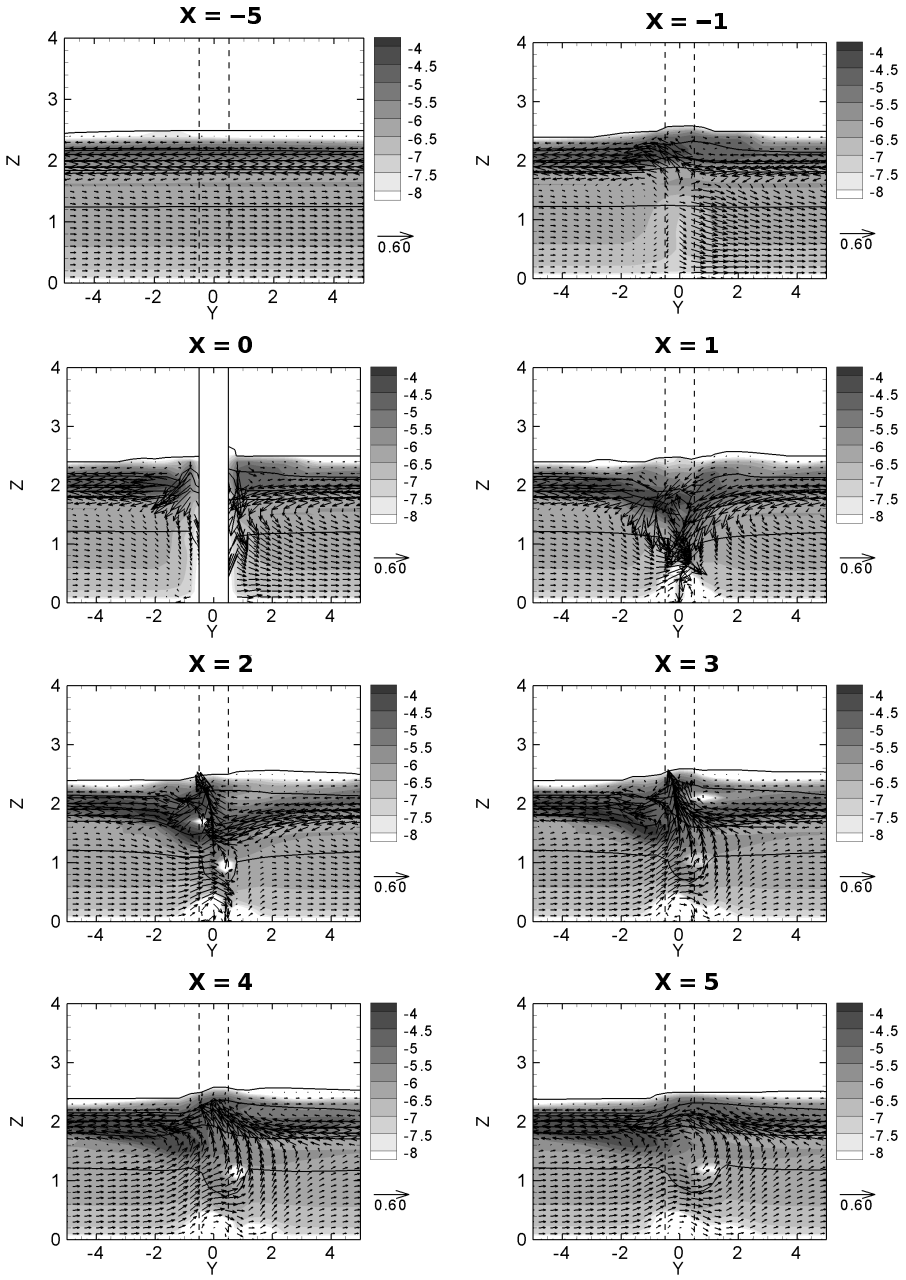

Figure 13: Flow field at different cross-sections in front of and behind the cylinder for the reference case 1121 ($D/d = 2$, $F_r = 0.57$, $K = 0.92$) with Coriolis forces. The grey scale indicates the decadal logarithm of the buoyancy production which is here a measure for the vertical mixing of salinity. X indicates the distance from individual cross-sections (in multiples of the cylinder diameter) from the centre of the cylinder, in front of (negative numbers) and behind the cylinder (positive numbers). The figure has been taken from Schimmels (2007).

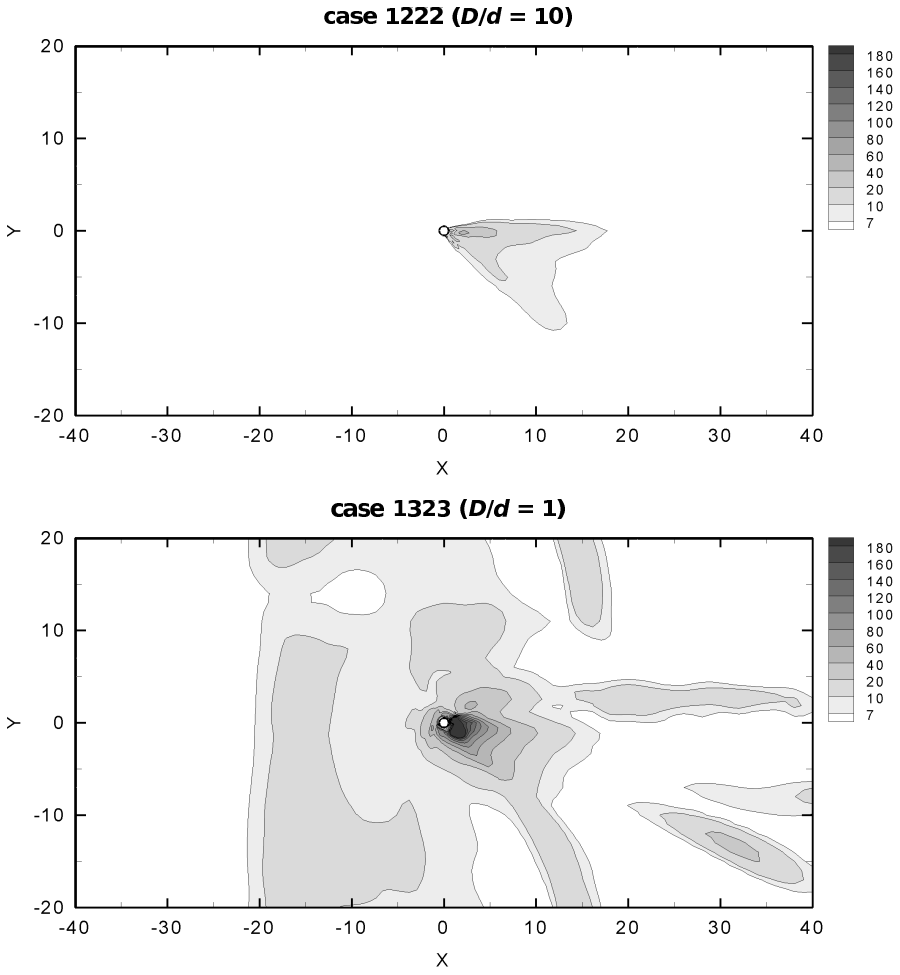

Figure 14: Influence of depth to diameter ratio, D/d on the entrainment rate for cases with constant Froude and Ekman number ($F_r = 0.57$, $K = 0.92$). The grey scale indicates the entrainment rate (to be multiplied by 10^5). The figure has been taken from Schimmels (2007).

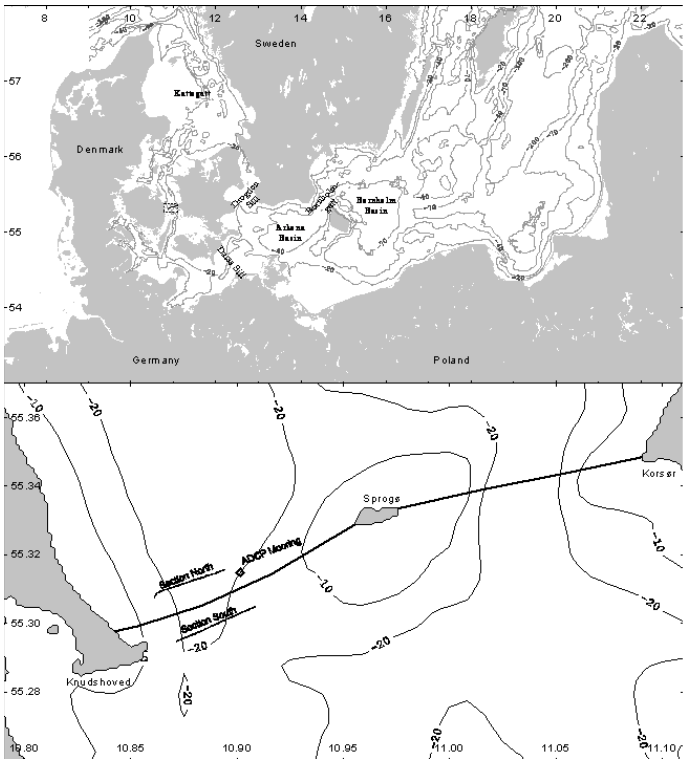

Figure 15: Maps of southern Baltic and the transition zone to the North Sea (upper panel and of the Great Belt Link (GBL) (lower panel). Depth contours are given in meters. The positions of characteristic sections of classical and towed CTD (conductivity-temperature-depth) as well as of dissipation profiler are indicated as lines. The figure has been taken from Lass et al. (2008).

surements during the first cruise. No variability of salinity was observed upstream of the bridge with a spatial scale of the distance between the two bridge piles, while pulse like variability with a scale of 70 m was observed 500 m downstream of the bridge, see figure 18.

It will be attempted in the near future to use these observations as one data set for the calibration of the structure mixing parameterisation discussed in section 4.

4 Parameterisation of structure mixing

4.1 Underlying physics

The friction due to structures in the water column is parameterised by a quadratic friction law, with the friction coefficient depending on the size, the shape and also on the number of structures in the flow. Taking the u-velocity (eastwards) and v-velocity (northwards) equations as they are implemented in the General Estuarine Transport Model (GETM), the terms written

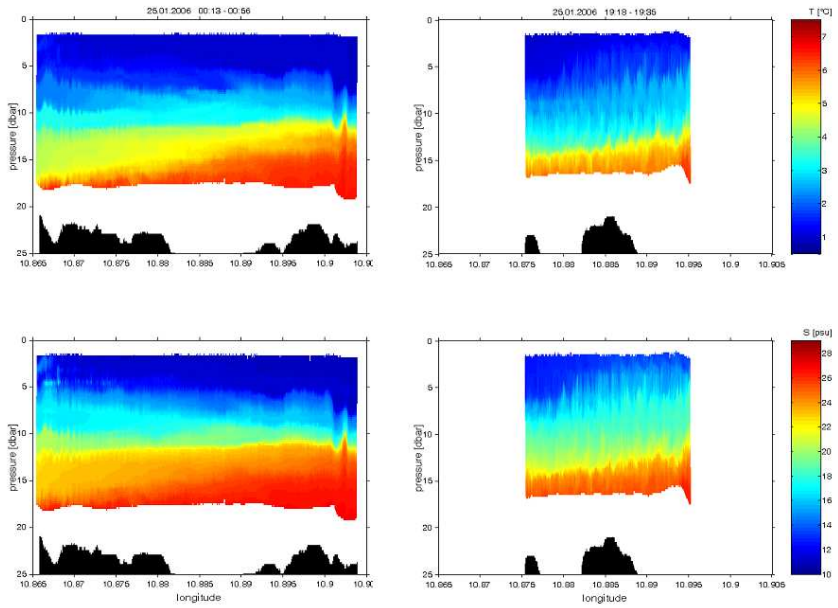

Figure 16: Left panels: Temperature and salinity measured by the towed CTD-chain on 25 January 2006 00:13 to 00:56 north of the western GBL. Right panels: Temperature and salinity measured by the towed CTD-chain on 25 January 2006 19:18 to 19:35 south of the western GBL. The figure has been taken from Lass et al. (2008).

in red are the additional terms for the structure friction:

$$\begin{aligned}\partial_t u + \partial_x(u^2) + \partial_y(uv) + \partial_z(uw) - \partial_z\left((\nu_t+\nu)\partial_z u\right) - fv + Cu\sqrt{u^2+v^2} \\ = -g\partial_x\zeta + \int_z^\zeta \partial_x b\, dz',\end{aligned} \tag{3}$$

$$\begin{aligned}\partial_t v + \partial_x(vu) + \partial_y(v^2) + \partial_z(vw) - \partial_z\left((\nu_t+\nu)\partial_z v\right) + fu + Cv\sqrt{u^2+v^2} \\ = -g\partial_y\zeta + \int_z^\zeta \partial_x b\, dz'.\end{aligned} \tag{4}$$

with the friction coefficient

$$C(z) = c(z)I(z). \tag{5}$$

For the meaning of the individual terms, in equations (3) and (4), see Burchard and Bolding (2002). In (5), c is a non-dimensional friction parameter depending on the shape and distribution of the structure (and probably also on the flow properties), and I is the diameter the structures

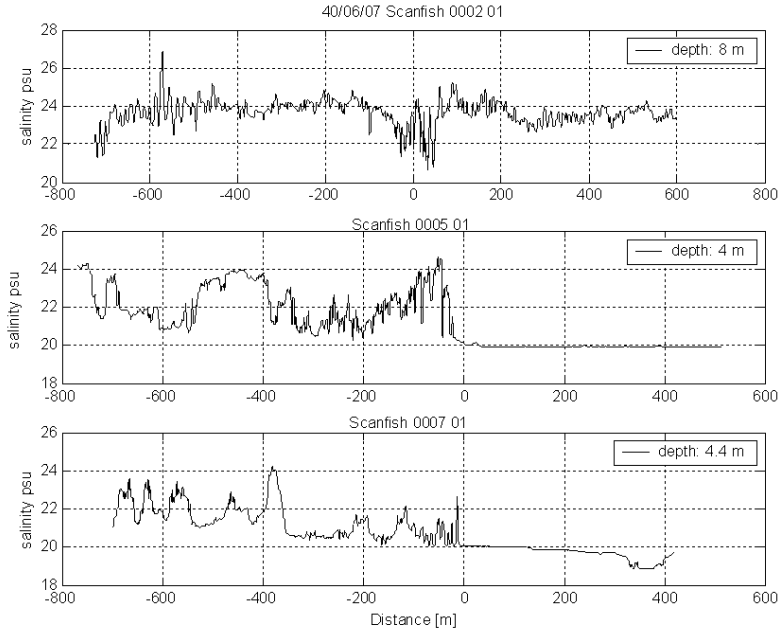

Figure 17: Salinity in the surface mixed layer measured with the Scanfish-CTD towed at a given depth level in meridional direction beneath the western GBL. The distance of the Scanfish is given with respect to the middle line of the GBL. The measurements in the upper panel were performed on 4 April 19:08, in the middle panel on 5 April 13:54, and in the lower panel on 5 April 14:48 UTC, respectively. The figure has been taken from Lass et al. (2008).

projected to the actual current direction per area for each depth. When calculating the mean kinetic energy equation, one will see that the loss of mean flow kinetic energy to turbulence is

$$P_c = \nu_t \left((\partial_z u)^2 + (\partial_z v)^2 \right) + C \left(u^2 + v^2 \right)^{3/2}, \tag{6}$$

where the first term on the right hand side is the shear production of turbulence and the second term is the contribution due to structure friction.
In a first-order approach, this should be included as an additional source term into the dynamic equation for the turbulent kinetic energy. By doing so, energy would be conserved when transferred from the mean flow to the turbulent regime. The increased turbulence would then result in increased vertical mixing, thus converting the additional turbulence into an additional increase of potential energy.
For a cylinder with constant diameter, we could as a first approximation assume that the parameter c is independent of the position in the water column, such that we have to optimise only one parameter by means of laboratory studies (University of Rostock), non-hydrostatic near-field studies (University of Hannover) and field observations at the Great Belt Bridge (IOW), see section 3 for details.

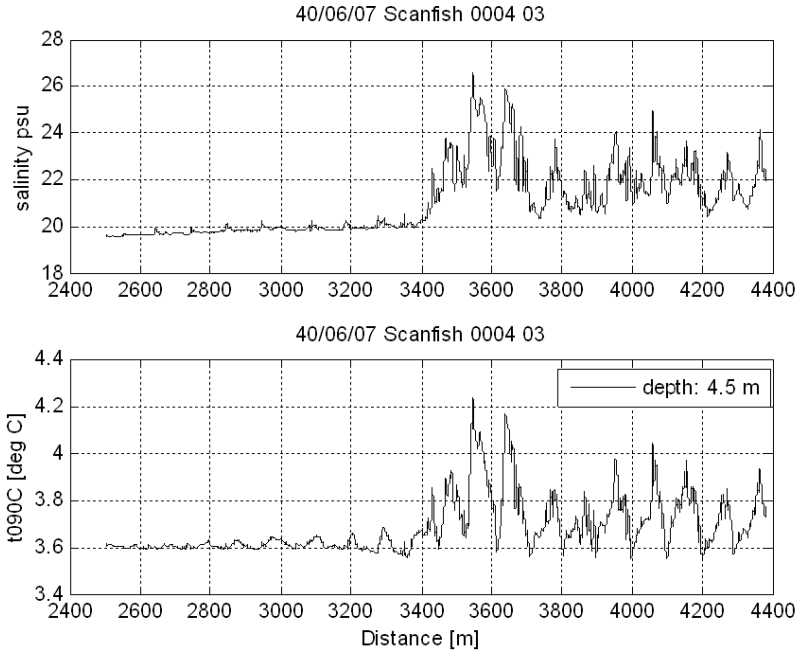

Figure 18: Salinity (upper panel) and temperature (lower panel) in the surface mixed layer measured at 5 April 2006 12:04 UTC with the Scanfish-CTD towed at a given depth level downstream of the western GBL. The distance of the Scanfish is given with respect to the western end of the GBL. The figure has been taken from Lass et al. (2008).

4.2 Calibration strategy

The calibration for the wind farm mixing parameterisation will mainly be based on the numerical experiments carried out by Schimmels (2007), see also section 3.2. For the rotational case with a Froude number of 0.57 and an Ekman number of 0.92 he simulated flow around cylinders with three different diameters, $D/d = 1$, $D/d = 2$, and $D/d = 10$ with the diameter d and the plume thickness D, see figures 13 and 14. With the domain of calculation being always 40 × 80 cylinder diameters, Schimmels (2007) obtained domain integrated entrainment rates of 0.168, 0.119 and 0.009, respectively, see his table 8.4. Related to the same absolute area of 400 m × 800 m the total entrainment of one cylinder for this area would thus result in 0.168, 0.02975 and $9.0 \cdot 10^{-5}$, respectively, or averaged over the whole 400 m × 800 m domain, $5.25 \cdot 10^{-5}$, $9.3 \cdot 10^{-6}$ and $2.81 \cdot 10^{-8}$, respectively. When placing four cylinders of diameter $D/d = 2$ and 10 cylinders of diameter $D/d = 10$ into the 400 m × 800 m domain, these two cases result in the same amount of projected cylinder area than for the case with one cylinder of diameter $D/d = 1$. Thus, for these three cases, we would expect average entrainment rates of $5.25 \cdot 10^{-5}$, $3.71 \cdot 10^{-5}$ and $2.81 \cdot 10^{-7}$. The reason for these differences are clearly seen in figure 13: The eddies behind the cylinder which scale with the cylinder diameter interact with the background flow which scales with the thickness of the dense bottom current. Therefore, the interaction of

the cylinder with the background flow is qualitatively different for different cylinder diameters. This does clearly mean that the friction coefficient c in equation (5) would have to be a function of D/d. Since for a general flow situation a thickness of the dense bottom current may not clearly be defined, the quantity d must not be used for the parameterisation. Instead, it would be an option to use the macro length scale of the turbulence, L, which would scale with the plume thickness, and would also be available for currents with completely different flow structures, since it is integral part of the underlying turbulence closure models.
It can furthermore be assumed from Schimmels (2007) that the calibration would also have to depend on the Froude number and the Ekman number of the flow.

5 First conclusions for the dynamic impact of offshore wind farms

Here, we try a first careful estimate for the impact of offshore wind farms on mixing in dense bottom currents. Since a calibration of the wind farm parameterisation presented in section 4 is not yet possible, realistic model simulations cannot be used for this. Therefore, let us assume the worst case of an elongated channel with a steady-state dense bottom current and a relatively dense wind farm. Using the channel north of Kriegers Flak as a rough orientation, we assume a 20 km long flat bottom channel of 40 m water depth covered with a 10 m thick dense bottom current with a salinity of 20 g/kg travelling with a current speed of 0.5 m/s. Overlying ambient water should be at rest with a salinity of 8 g/kg. With these specifications, the situation is close to the observations by Sellschopp et al. (2006), Arneborg et al. (2007) and Umlauf et al. (2007), as well as the local model experiments by Schimmels (2007) which are discussed in section 3.2.
Let us further assume that the considered area is completely covered with a wind farm consisting of cylindric wind turbines of a diameter of 10 m and a spacing of 400 m $\times$ 800 m. This is comparable to the numerical experiment 1323 by Schimmels (2007), see figure 14. For this case, Schimmels (2007) estimated an additional entrainment caused by the cylinder of 0.168 per 400 m $\times$ 800 m area, resulting in an average cylinder entrainment of $5.25 \cdot 10^{-5}$. With a background natural entrainment of $3.2 \cdot 10^{-5}$, the total entrainment rate for the wind farm would be $8.45 \cdot 10^{-5}$. With the dense bottom current velocity of 0.5 m/s, the entrainment velocity would be $4.425 \cdot 10^{-5}$ m/s with wind turbines and $1.6 \cdot 10^{-5}$ m/s without wind turbines. For the idealised case considered here, the passage time for the dense bottom current would be 40.000 s for the 20 km long domain. Assuming constant entrainment velocities, the total entrainment (increase of thickness of dense bottom currents) would therefore be 1.77 m with wind turbines and 0.64 m without wind turbines. Therefore, assuming total salt conservation, after the passage through the 20 km long area the dense bottom current subject to wind farm mixing would have a reduced salinity of 18.20 g/kg whereas the dense bottom current salinity without wind turbines would have reduced to 19.28 g/kg.
Thus the additional salinity loss due to a wind farm would be nearly 1 g/kg, a value which surely would have a dynamic effect when the bottom current is further propagating towards deeper basins.
For this rough estimate, a kind of worst case scenario has been chosen, with a very dense wind farm in a critical area. But given the large uncertainty of the entrainment calculations

by Schimmels (2007), also a more realistic wind turbine spacing could result in a detectable reduction of salinity of dense bottom currents.
Whereas a doubling of wind turbine spacing in both directions (resulting in a 800 m × 1600 m spacing) would reduce the salinity loss to a fourth, changing the type of wind turbine foundation could significantly change the mixing and subsequent salinity loss. Gravity foundations which have been discussed for large wind turbines would be founded on large concrete structures the effect of which on the entrainment may be much higher than the effect of cylindric structures.
Placements of wind farms in regions with strong and frequent dense bottom currents may be critical. Far less critical will be the location of wind farms in areas with low current velocities (such as in the centre of the Arkona Sea) or in areas which are mostly well-mixed (in shallow areas of less than 20 m water depth).
The way forward towards more reliable estimates of wind farm mixing will be to substantially increase the number of experiments with the model of Schimmels (2007) in order to properly calibrate the friction parameterisation. The results of Schimmels (2007) need to be compared at least qualitatively with the laboratory experiments carried out within the QuantAS-Off project by the University of Rostock for a variety of Froude numbers. It would also be very helpful, if the local numerical experiments by the University of Hannover would consider one or two different shapes of structures such as gravity foundations or semi-diving constructions.
Once a proper calibration for wind farm mixing is available, model experiments will be carried out with the Western Baltic Sea model by Burchard et al. (2008), with various realistic distributions of wind farms.

References

Arneborg, L., V. Fiekas, L. Umlauf, and H. Burchard, 2007: Gravity current dynamics and entrainment - a process study based on observations in the Arkona Basin. *J. Phys. Oceanogr.*, **37**, 2094–2113.

Burchard, H. and K. Bolding, 2002: GETM – a general estuarine transport model. Scientific documentation. Tech. Rep. EUR 20253 EN, European Commission.

Burchard, H., F. Janssen, K. Bolding, L. Umlauf, and H. Rennau, 2008: Model simulations of dense bottom currents in the Western Baltic Sea. *Cont. Shelf Res.*, in print.

Burchard, H., H. Lass, V. Mohrholz, L. Umlauf, J. Sellschopp, V. Fiekas, K. Bolding, and L. Arneborg, 2005: Dynamics of medium-intensity dense water plumes in the Arkona Sea, Western Baltic Sea. *Ocean Dynamics*, **55**, 391–402.

Burchard, H. and H. Rennau, 2008: Comparative quantification of physically and numerically induced mixing in ocean models. *Ocean Modelling*, **20**, 293–311.

Feistel, R., G. Nausch, and E. Hagen, 2006: Unusual Baltic inflow activity 2002/3 and varying deep-water properties. *Oceanologia*, **48**, 21–35.

Feistel, R., G. Nausch, T. Heene, J. Piechura, and E. Hagen, 2004: Evidence for a warm water inflow into the Baltic Proper in summer 2003. *Oceanologia*, **46**, 581–598.

Feistel, R., G. Nausch, V. Mohrholz, E. Lysiak-Pastuszak, T. Seifert, W. Matthäus, S. Krüger, and I. S. Hansen, 2003: Warm waters of summer 2002 in the deep Baltic Proper. *Oceanologia*, **45**, 571–592.

Griffies, S. M., R. C. Pacanowski, M. Schmidt, and V. Balaji, 2001: Tracer Conservation with an Explicit Free Surface Method for z-Coordinate Ocean Models. *Mon. Weather Rev.*, **129**, 1081–1098.

Janssen, F., T. Neumann, and M. Schmidt, 2004: Inter-annual variability in cyanobacteria blooms in the Baltic Sea controlled by wintertime hydrographic conditions. *Mar. Ecol. Prog. Ser.*, **275**, 59–68.

Kõuts, T. and A. Omstedt, 1993: Deep water exchange in the Baltic Proper. *Tellus*, **45 A**, 311–324.

Lass, H. U. and W. Matthäus, 1996: On temporal wind variations forcing salt water inflows into the Baltic Sea. *Tellus*, **48 A**, doi:10.1034/j.1600–0870.1996.t01–4–00 005.x.

Lass, H. U. and V. Mohrholz, 2003: On the dynamics and mixing of inflowing salt-water in the Arkona Sea. *J. Geophys. Res.*, **108**, 3042, doi: 10.1029/2002JC001 465.

Lass, H. U., V. Mohrholz, M. Knoll, and H. Prandke, 2008: On the impact of a pile on a moving stratified flow. *J. Mar. Sys.*, accepted for publication.

Lass, H. U., V. Mohrholz, and T. Seifert, 2005: On pathways and residence time of saltwater plumes in the Arkona Sea. *J. Geophys. Res.*, **110**, doi:10.1029/2004JC002 848.

Lehmann, A., P. Lorenz, and D. Jacob, 2004: Modelling the exceptional Baltic Sea inflow events in 2002-2003. *Geophys. Res. Lett.*, **31**, doi:10.1029/2004GL020 830.

Liljebladh, B. and A. Stigebrandt, 1996: Observations of the deepwater flow into the Baltic Sea. *J. Geophys. Res.*, **101**, 8895–8911.

Matthäus, W. and H. Frank, 1992: Characteristics of major Baltic inflows – a statistical analysis. *Cont. Shelf Res.*, **12**, 1375–1400.

Meier, H. E. M., R. Döscher, A. C. Coward, J. Nycander, and K. Döös, 1999: RCO - Rossby Centre regional Ocean climate model: model description (version 1.0) and first results from the hindcast period 1992/93. Tech. Rep. Reports Oceanography No. 26, Swedish Meteorological and Hydrological Institute, Norrköping, Sweden.

Menzel, P., F. Hüttmann, M. Brede, and A. Leder, 2007: Experimental investigations of mixing-processes in the wake of a circular cylinder in stratified flows. *AIP Conf. Proc.*, 914.

Menzel, P., F. Richter, and A. Leder, 2006: Schichtkanal zur Untersuchung von Mischungsvorgängen in geschichteten Strömungen hinter einem Kreiszylinder mittels PIV/PLIF. *Lasermethoden in der Strömungsmesstechnik 14. Fachtagung der GALA e.V. 2006*, Dopheide, D., H. Müller, V. Strunck, B. Ruck, and A. A. Leder, Eds., Braunschweig, 55.1–55.8.

Mohrholz, V., J. Dutz, and G. Kraus, 2006: The impact of exceptionally warm summer inflow events on the environmental conditions in the Bornholm Sea. *J. Mar. Sys.*, **60**, 285–301.

Neumann, T., W. Fennel, and C. Kremp, 2002: Experimental simulations with an ecosystem model of the Baltic Sea: A nutrient load reduction experiment. *Global Biogeochemical Cycles*, **16**, 10.1029/2001GB001 450.

Paka, V. T., V. M. Zhurbas, N. N. Golenko, and L. A. Stefantzev, 1998: Effect of the Ekman transport on the overflow of saline waters through the Slupsk Furrow in the Baltic Sea. *Izv. Atmos. Ocean. Phys.*, **34**, 641–648, translated from Izvestija AN. Fizika Atmosfery i Okeana, vol. 43, No. 5, 1998, 713-720.

Reissmann, J. H., H. Burchard, R. Feistel, E. Hagen, H. U. Lass, V. Mohrholz, G. Nausch, L. Umlauf, and G. Wieczorek, 2008: State-of-the-art review on Baltic mixing and consequences for eutrophication. *Progr. Oceanogr.*, in print.

Schimmels, S., 2007: Numerical simulation of the influence of circular cylinders on mixing and entrainment in natural density currents. Ph.D. thesis, Fluid Mechanics Institute, Leibniz University of Hannover, Germany.

Sellschopp, J., L. Arneborg, M. Knoll, V. Fiekas, F. Gerdes, H. Burchard, H. U. Lass, V. Mohrholz, and L. Umlauf, 2006: Direct observations of a medium-intensity inflow into the Baltic Sea. *Cont. Shelf Res.*, **26**, 2393–2414.

Umlauf, L., L. Arneborg, H. Burchard, V. Fiekas, H. U. Lass, V. Mohrholz, and H. Prandke, 2007: The transverse structure of turbulence in a rotating gravity current. *Geophys. Res. Lett.*, **34**, L08 601, doi:10.1029/2007GL029 521.

Wyrtki, K., 1954: Der große Salzeinbruch in die Ostsee im November und Dezember 1951. *Kieler Meeresforsch.*, **10**, 19–25.